Advances in
HEAT
TRANSFER

Serial Editors

James P. Hartnett
Energy Resources Center
University of Illinois
Chicago, Illinois

Thomas F. Irvine, Jr.
Department of Mechanical Engineering
State University of New York at Stony Brook
Stony Brook, New York

Serial Associate Editor
Young I. Cho
Department of Mechanical Engineering and Mechanics
Drexel University
Philadelphia, Pennsylvania

Volume 24

Contributors to this Volume

B. S. Bačlić
Adrian Bejan
Jae Min Hyun
A. V. Shenoy
Wei Shyy
B. D. Vujanović

Advances in
HEAT
TRANSFER

Volume 24

CONTENTS

Contact Melting Heat Transfer and Lubrication

ADRIAN BEJAN

Variational Solutions of Transient Heat Conduction Through Bodies of Finite Length

B. D. VUJANOVIĆ AND B. S. BAČLIĆ

The serial publication *Advances in Heat Transfer* is designed to fill the information gap between the regularly scheduled journals and university-level textbooks. The general purpose of this publication is to present review articles or monographs on special topics of current interest. Each chapter starts from widely understood principles and brings the reader up to the forefront of the topic in a logical fashion. The favorable response by the international scientific and engineering community to the volumes published to date is an indication of how successful our authors have been in fulfilling this purpose.

The Editors are pleased to announce the publication of Volume 24 and wish to express their appreciation to the current authors, who have so effectively maintained the spirit of this serial publication.

Contact Melting Heat Transfer
and Lubrication

ADRIAN BEJAN

J. A. Jones Professor of Mechanical Engineering
Duke University
Durham, North Carolina

I. Introduction

The subject of this review is the relatively recent work on melting and lubrication at the interface between two solid parts, one of which is at its melting point. It is an area of research that began in heat transfer, with studies of contact melting inside capsules (Section II) and around embedded objects (Section III). Melt lubrication is now a distinct topic in tribology (Pinkus [1]).

The classical application of melt lubrication is in the area of sliding friction on ice and snow. Among the more modern applications is the coating of a metallic part with another metal whose melting point is considerably lower. The function of the latter is to melt and serve as lubricant in a

1

manufacturing process to which the former may be subjected. Another application is in the field of interior ballistics, where a projectile (e.g., brass bullet) melts superficially as it travels along a gun barrel (Aung [2]). Other applications include the storage of energy as latent heat inside capsules and the burial of heat-generating bodies.

The research reviewed in this chapter covers the contract melting of crystalline substances, anomalous crystalline substances such as ice, and the contact softening of glass-like substances. These occur in diverse contact region geometries. The shapes of the mating solid surfaces may be concave, convex, or plane, while the perimeter of plane contact regions may be either rectangular or circular. The types of relative motion reviewed here are sliding contact, rolling contact, the movement of a hot body through a melting solid medium, and the movement of a solid melting inside a heated capsule. The effect the roughness, or contact melting over the tops of asperities, is also analyzed.

II. Contact Melting Inside a Heated Capsule

Figure 1 shows the geometry in which the phenomenon of close-contact melting has been studied the most thoroughly. Initially, the solid phase-change material fills a space (capsule) shaped as a sphere or a horizontal cylinder. Beginning with a certain point in time, heating is applied through the wall of the capsule while melting occurs in a thin film all around the solid. If the density of the solid is greater than the density of the liquid, the shrinking solid sinks to the bottom while continuing to experience contact melting by pressing against the capsule wall. The liquid accumulates in the
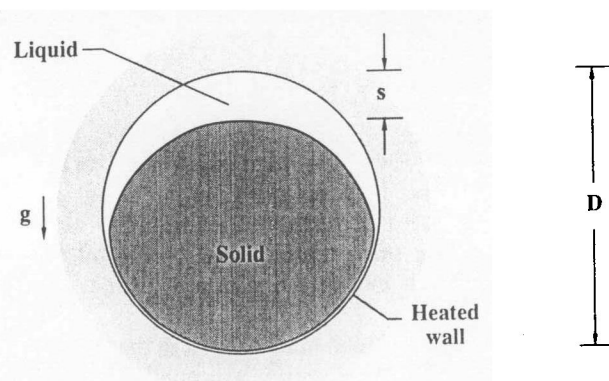
Fig. 1. Close-contact melting inside a capsule shaped as a sphere or horizontal cylinder.

larger space created above the solid. The melting on the upper surface of the solid is not nearly as intense as on the lower (close-contact) surface, even though natural convection currents are present throughout the upper liquid.

The name, *close contact melting*, is somewhat deceiving, because the solid never comes in direct contact with the heated wall. A liquid film with finite thickness always bridges the temperature gap between the wall and the solid (the melting front). The liquid generated at the melting front is squeezed out from under the solid by the higher pressure maintained in the central section of the film by the weight of the free solid. In this way the film supports the solid, and every feature of the melting process (film thickness, melting rate) depends on the geometry (shape, size) of the shrinking solid.

Nicholas and Bayazitoglu [3] were the first to study close-contact melting as a distinct and important mechanism during melting inside a capsule in which the solid is free to migrate. This was an important step because melting inside capsules had been studied extensively in circumstances where conduction was the only heat transfer mechanism (e.g., Shamsundar and Sparrow [4], and Katayama *et al.* [5]), or where the shrinking solid was supported in the center of the capsule (e.g., Pannu *et al.* [6], Saitoh and Hirose [7], Rieger *et al.* [8], and Ho and Viskanta [9]). Nicholas and Bayazitoglu [3] considered horizontal cylinder geometry, and determined numerically the flow and temperature fields in the liquid regions and the changing shape of the solid. Spherical geometry was studied numerically and experimentally in a follow-up paper (Moore and Bayazitoglu [10]).

Of special interest to the melt lubrication work reviewed later is the analytical modeling of close-contact melting inside a capsule. For horizontal cylinders this was done by Bareiss and Beer [11], Prasad and Sengupta [12, 13], and Saito *et al.* [14]. Spherical geometry was analyzed by Roy and Sengupta [15, 16] and Bahrami and Wang [17]. As summarized by Roy and Sengupta [16], the main features of the analytical model are as follows:

(a) The process is quasi-steady, i.e., at every point in time the weight of the solid is balanced by the excess pressure built in the liquid film;
(b) Heat transfer through the liquid film is by pure conduction in the radial direction, and no melting occurs on the upper surface of the solid;
(c) The process is axisymmetric, with Poiseuille-type flow in the close-contact gap, i.e., there is no slip at the capsule wall or at the melting front;
(d) The pressure at the two openings of the close-contact gap is equal to the hydrostatic pressure in the upper pool of liquid;
(e) The area of the melting front is taken as approximately equal to the area of the mating portion of the capsule wall;

FIG. 2. History of melting rate and fall of a solid in a horizontal cylindrical capsule with uniform wall temperature (drawn based on Bareiss and Beer solution [11]).
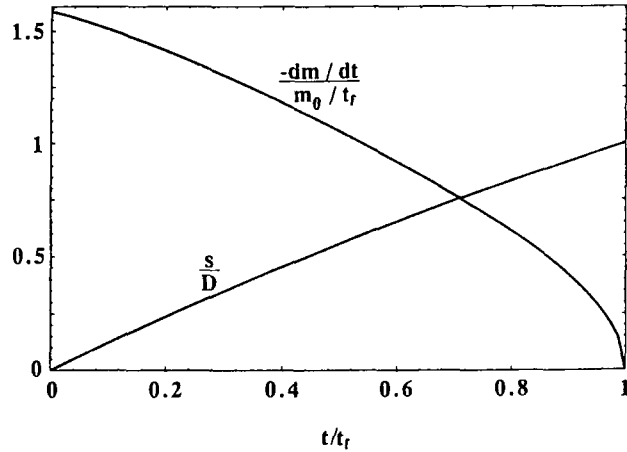
(f) The shear stress experienced by the solid as it drops and sweeps the lateral wall is negligible.

The analytical solution obtained by Bareiss and Beer [11] for melting inside a horizontal cylinder is summarized in Fig. 2. Initially the solid is at the melting point (T_m), and fills the cylinder. The wall temperature is raised to T_w at the time $t = 0$. The time t_f needed to melt all the solid is given by the dimensionless expression

$$\frac{\alpha t_f}{R^2} = 2.49\left(\frac{\rho}{\rho_s}\text{Ste}\right)^{-3/4}(\text{Pr Ar})^{-1/4}(1 + C)^{-1}, \qquad (1)$$

where $\text{Pr} = \nu/\alpha$, and

$$\text{Ste} = \frac{c_P(T_w - T_m)}{h_{sf}}, \qquad (2)$$

$$\text{Ar} = \left(1 - \frac{\rho}{\rho_s}\right)\frac{gR^3}{\nu^2}. \qquad (3)$$

The term C is an empirical correction introduced to account for additional melting associated with natural convection over the upper surface of the solid,

$$C = 0.25\left(\frac{\rho}{\rho_s}\text{Ste}\frac{\text{Ra}}{\text{Pr Ar}}\right)^{1/4}, \qquad (4)$$

in which $\text{Ra} = g\beta(T_w - T_m)D^3/\alpha\nu$. The effect of natural convection was documented in greater detail by Said and Sengupta [18] and Prasad and Sengupta [12, 13], based on numerical simulations.

The curve labeled s/D in Fig. 2 shows the distance traveled by the original geometric center of the solid in the downward direction. This distance is the same as the largest liquid gap $s(t)$ at the top of the solid (Fig. 2) when melting over the upper surface of the solid is negligible. The figure shows that the solid "falls" at a nearly uniform speed D/t_f, since $s(t)$ increases almost linearly from $s(0) = 0$ to $s(t_f) = D$.

The curve labeled $(-dm/dt)/(m_0/t_f)$ in Fig. 2 shows the history of the melting rate $(-dm/dt)$. The instantaneous mass of the solid is $m(t)$, and the initial mass is $m(0) = m_0$. The denominator m_0/t_f is the melting rate averaged over the entire duration of the process. The figure shows that in the early stages, when the solid is almost round, the melting rate is about 50% greater than the t_f-averaged melting rate.

Roy and Sengupta [15, 16] and Bahrami and Wang [17] reported thin-film analyses for contact melting in a spherical enclosure. Roy and Sengupta's results are presented as a family of curves with Ste/Pr and $\text{Ar}/(\rho/\rho_s)$ as independent parameters. The predicted melting rate agrees well with Moore and Bayazitoglu's [10] experiments with n-octadecane. In addition, the analysis shows that the contact melting film is thinner at the lowest point of the spherical surface and that the melting rate decreases as $\text{Ar}/(\rho/\rho_s)$ decreases. Bahrami and Wang [17] developed a closed-form expression for the time interval needed to melt all the solid. If we use the definition of Ar given in Eq. (3), Bahrami and Wang's [17] expression is rewritten as

$$\frac{\alpha t_f}{R^2} = 2.03\left(\frac{\rho}{\rho_s}\text{Ste}\right)^{-3/4}(\text{Pr Ar})^{-1/4}. \qquad (5)$$

This can now be compared to Eq. (1) for the cylindrical capsule, leading us to conclude that the melting time inside the spherical capsule is 18% shorter. The gradual fall of the solid is described by a s/D versus t/t_f curve that is nearly the same as the curve shown in Fig. 2 for melting inside a horizontal cylinder. In other words, the downward velocity of the solid is essentially constant over time, regardless of the shape of the capsule.

Experimental observations of the melting of ice in a horizontal cylindrical capsule were reported by Webb et al. [19]. The ice rises and experiences contact melting over the top surface. If the wall temperature is less than the density inversion temperature (4 °C), the liquid flow pattern is similar to the upside-down image of the flow of liquid paraffin. When the wall temperature is considerably greater than 4 °C, the water flow is two-dimensional in the two horn-shaped corners (near the exits from the contact melting gap),

and three-dimensional in the central portion. At wall temperatures close to 4 °C, the flow pattern is transitional, with several two-dimensional rolls. The measured melting rates agree well with predictions based on Bareiss and Beer's [11] analysis.

Contact melting was observed also inside a cylindrical capsule whose axis is tilted with respect to the vertical direction (Sparrow and Myrum [20]). Another basic geometry is the contact melting of a block of phase-change material pressed against a flat heater. This was studied experimentally by Saito *et al.* [21], numerically by Saito *et al.* [22] and Nagakubo and Saito [23], and experimentally and analytically by Moallemi *et al.* [24] and Hirata *et al.* [25]. Flat film geometry will be discussed in Section IV, as it is a special case (no relative motion, $U = 0$) of the melt lubrication problem outlined in Fig. 4. Contact melting in an inclined rectangular enclosure was studied experimentally and numerically by Saito *et al.* [26].

III. Sinking of a Hot Object Embedded in a Solid Phase-Change Material

If we turn the geometry of Fig. 1 inside out we arrive at Fig. 3, which shows how a hot object sinks into a larger body of solid phase-change material. Contact melting occurs over the leading portion of the hot object,
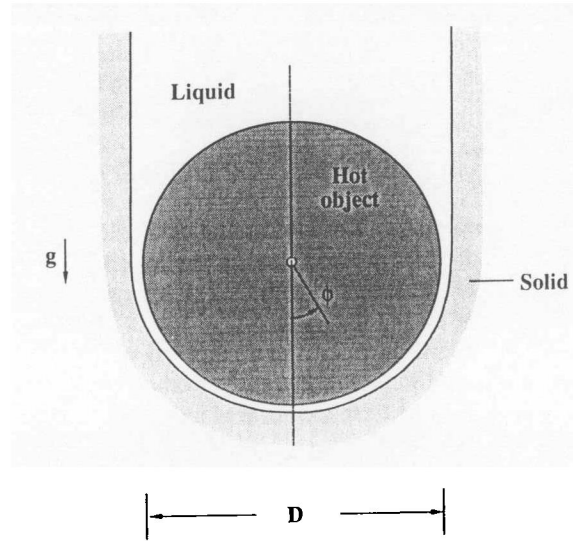
FIG. 3. External contact melting: heated sphere or horizontal cylinder sinking through a solid phase-change material.

the pressure built in the liquid film supporting the weight of the object during its quasi-steady sinking motion. The liquid wake generated behind the object refreezes at some distance downstream if the solid phase-change material is subcooled.

The earliest description of contact melting around embedded objects appears to have been reported by Nye [27]. His analysis dealt with unheated objects embedded in ice, where melting is due to pressure, i.e., the decrease of the melting point of ice as pressure under the object increases. This phenomenon will be discussed in Section XI.

Emerman and Turcotte [28] studied the motion of a heated sphere (T_w) through a solid phase-change material whose temperature T_∞ is below its melting point (T_m). They found that the liquid film thickness $\delta(\phi)$ must increase dramatically in the direction pointing away from the "nose" of the sphere ($\phi = 0$),

$$\delta(\phi) = \frac{\alpha \, \text{Ste}}{V \cos \phi}, \qquad (\text{Ste} \ll 1) \qquad (6)$$

where the Stefan number

$$\text{Ste} = \frac{c_P(T_w - T_m)}{h'_{sf}} \qquad (7)$$

is based on the augmented latent heat of melting

$$h'_{sf} = h_{sf} + c_s(T_m - T_\infty). \qquad (8)$$

The vertical velocity of the sphere V is proportional to the imposed temperature difference ($T_w - T_m$) raised to the power 3/4. If the Stefan number is much smaller than 1, the velocity is given by

$$\frac{VR}{\alpha} = \text{Ste}^{3/4}\left(\frac{8}{3} \cdot \frac{g \, \Delta\rho \, R^3}{\mu\alpha}\right)^{1/4} \qquad (\text{Ste} \ll 1), \qquad (9)$$

in which $\Delta\rho$ is the difference between the density of the object (sphere) and the density of the surrounding melt, $\Delta\rho = \rho_0 - \rho$. The same result for V can be expressed in terms of the volumetric rate of internal heat generation in the sphere, $\dot{q}$ (i.e., instead of in terms of the driving temperature difference $T_w - T_m$, or Ste),

$$V = \frac{4R\dot{q}}{3\rho h'_{sf}} \qquad (\text{Ste} \ll 1). \qquad (10)$$

The results summarized in Eqs. (6)–(10) are valid only for small Stefan numbers. More general results valid for any Ste value are given by Emerman and Turcotte [28].

The sinking of a horizontal cylinder embedded in a solid phase-change medium was studied experimentally and analytically by Moallemi and Viskanta [29, 30]. Their analytical results are valid for any Stefan number. In the Ste $\ll$ 1 limit, the film thickness varies according to Eq. (6) over the leading surface of the cylinder, while the vertical velocity V is given by

$$\frac{VR}{\alpha} = \mathrm{Ste}^{3/4}\left(\frac{5\pi}{16} \cdot \frac{g\,\Delta\rho\,R^3}{\mu\alpha}\right)^{1/4} \qquad (\mathrm{Ste} \ll 1). \qquad (11)$$

The similarities between Eqs. (11) and (9) are self-evident. The differential numerical coefficients on the right-hand side show that the velocity of the sinking sphere is 28% greater than the velocity of a horizontal cylinder with the same diameter. The design problem of optimizing the shape of the embedded object was treated by Fomin and Cheng [31].

It is interesting to note that contact melting around embedded hot objects agrees in a scaling sense with contact melting inside heated capsules. For example, the average vertical velocity of the solid in the capsule of Fig. 1 is

$$\bar{V} = \frac{D}{t_\mathrm{f}} \qquad (12)$$

for which the t_f scale is furnished by Eq. (1). If in Eq. (1) we neglect factors of order 1 (cf., the rules of scale analysis, Bejan [32]), namely $D/R \sim O(1)$, $(1 + C) \sim O(1)$, $(\rho/\rho_\mathrm{s}) \sim O(1)$, and $2.49 \sim O(1)$, we obtain in place of Eq. (12)

$$\frac{\bar{V}R}{\alpha} \sim \mathrm{Ste}^{3/4}\left(\frac{g\,\Delta\rho\,R^3}{\mu\alpha}\right)^{1/4}. \qquad (13)$$

In this equation $\Delta\rho$ is the density difference between the solid which sinks in Fig. 1 and the surrounding fluid, i.e., $\Delta\rho = \rho_\mathrm{s} - \rho$. The order of magnitude identity between Eq. (13) and Eqs. (9)–(11) demonstrates the analogy between *internal* contact melting (Fig. 1) and *external* contact melting (Fig. 3). We shall expand on this observation in Section V.

IV. Sliding Contact Melting

The thin film of liquid maintained by contact melting can serve as lubricant when a wall slides past solid phase-change material [33–40]. The simplest geometry in which contact melting lubrication occurs is illustrated in Fig. 4 (Bejan [40]). A two-dimensional block of phase-change material of thickness L and length B (perpendicular to the figure) is pushed with normal force F_n against a solid slider. The melting rate, or speed at which the block advances into the slider, is V.
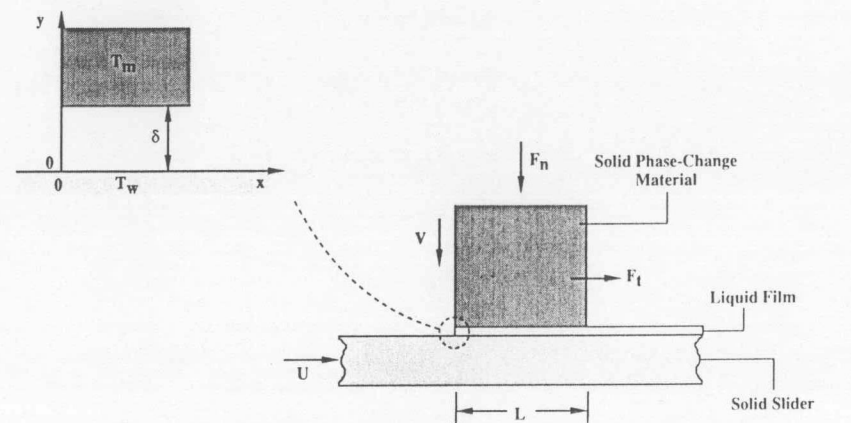

Fig. 4. Block of phase-change material pressed against a plane slider.

The relative translational speed between the two bodies is U and the tangential (friction) force is F_t. The solid phase-change material is at the melting point T_m, while the slider is at a higher temperature T_w. It is maintained at this higher level either by heating the slider externally, or by virtue of the heating effect caused by viscous dissipation in the liquid film. We shall examine both cases by means of scale analysis. The challenge is to predict the melting rate and the friction force as functions of the normal force and the relative speed.

The energy equation for the liquid film can be written with reference to the (x, y, z) frame shown in Fig. 4, in which (u, v, w) are the corresponding liquid velocity components,

$$\underbrace{u\frac{\partial T}{\partial x} + v\frac{\partial T}{\partial y} + w\frac{\partial T}{\partial z}}_{\boxed{\text{H2-ap ht24 10a}}} = \underbrace{\alpha\frac{\partial^2 T}{\partial y^2}}_{\boxed{\text{H2-ap ht24}}} + \underbrace{\frac{\mu}{\rho c_\mathrm{P}}\Phi}_{\boxed{\text{H2-ap ht2}}}. \qquad (14)$$

$$\underset{\text{convection}}{\frac{U\,\Delta T}{L}} \qquad \underset{\text{conduction}}{\alpha\frac{\Delta T}{\delta^2}} \qquad \underset{\substack{\text{viscous}\\\text{heating}}}{\frac{\mu}{\rho c_\mathrm{P}}\left(\frac{U}{\delta}\right)^2}$$

Equation (14) is based on the assumption that the film is very thin, $\delta \ll \min(B, L)$. Listed underneath the terms of the equation are the representative scales of the three effects that compete in the energy balance: convection, conduction, and internal heat generation.

The transversal conduction effect is always important, since without it there would be no melting at the $y = \delta$ interface. Convection is negligible

relative to conduction if $U \cdot \Delta T/L \ll \alpha \Delta T/\delta^2$, which means that

$$\left(\frac{\delta}{L}\right)^2 \frac{UL}{\alpha} \ll 1. \tag{15}$$

This holds true in most thermal film lubrication problems, since here the film is very thin, $(\delta/L) \ll 1$, and the Peclet number UL/α is finite.

The viscous heating effect is negligible with respect to transversal conduction when $(\mu/\rho c_P)(U/\delta)^2 \ll \alpha \Delta T/\delta^2$, which means that

$$\frac{\mu U^2}{k \Delta T} \ll 1, \tag{16}$$

where ΔT is the scale of the temperature difference $(T_w - T_m)$. It is interesting that the viscous dissipation criterion (16) does not depend on film thickness δ.

When conditions (15) and (16) are satisfied simultaneously, heat transfer in the liquid film is by pure conduction in a direction perpendicular to the film, in agreement with assumption (b) of the contact melting analyses reviewed in Section II. Viscous heating is negligible, while melting is caused entirely by the imposed temperature difference $(T_w - T_m)$, where T_w is the temperature of the isothermal slider. The sliding contact geometry of Fig. 4 was subjected to contact melting analysis by Bejan [40] under the additional assumption that $\rho_s \cong \rho$. One conclusion is that film thickness is uniform and independent of the speed U,

$$\frac{\delta}{L} = \left(\frac{\text{Ste}}{\Pi}\phi\right)^{1/4} \quad (\rho_s \cong \rho). \tag{17}$$

In this equation Π is the nondimensionalized version of the average excess pressure experienced by the film,

$$\Delta P = \frac{F_n}{BL}, \tag{18}$$

that is,

$$\Pi = \frac{\Delta P \cdot L^2}{\mu\alpha}. \tag{19}$$

The pressure drop number Π is an important dimensionless group which must be recognized in forced convection configurations in which the pressure difference is imposed (Bejan [41]). The factor ϕ accounts for the shape (ratio B/L) of the sliding contact area in Fig. 5. The asymptotes of the $\phi(B/L)$ curve are $\phi \to 1$ when $B/L \gg 1$, and $\phi \to (B/L)^2$ when $B/L \ll 1$.
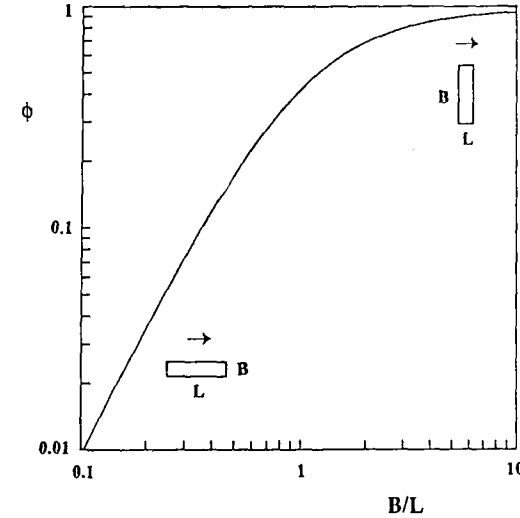
FIG. 5. Effect of aspect ratio of sliding contact area on film thickness (Eq. (17)), melting rate (Eq. (20)), and friction coefficient (Eq. (21)).

The corresponding result for the melting rate (Bejan [40]) can be arranged as in Eqs. (9) and (11):

$$\frac{VL}{\alpha} = \text{Ste}^{3/4}\left(\frac{\Delta P \cdot L^2}{\mu\alpha\phi}\right)^{1/4} \quad (\rho_s \cong \rho). \tag{20}$$

This, too, is independent of the slider speed U. The total tangential force is $F_t = \mu(U/\delta)BL$, which translates into the friction coefficient

$$\mu_f = \frac{F_t}{F_n} = \frac{UL}{\alpha}(\text{Ste } \phi)^{-1/4}\Pi^{-3/4} \quad (\rho_s \cong \rho). \tag{21}$$

In conclusion, the friction coefficient increases linearly with the tangential velocity U, and decreases as $L^{-1/2}$. It also decreases monotonically as the imposed excess pressure Π and temperature difference (Ste) increase.

V. Scale Analysis and Correlation of Contact Melting

This is a good opportunity to show that all the results on contact melting reviewed until now can be predicted based on scale analysis [42]. We continue to use the terminology of Fig. 4, but now write l for the longitudinal length scale of liquid flow through the film. We further assume that the

contact surface is not necessarily plane. The conservation of mass in the liquid film requires that

$$u\delta \sim Vl. \tag{22}$$

The momentum balance is simply

$$\frac{\Delta P}{l} \sim \mu\frac{u}{\delta^2}, \tag{23}$$

since shearing caused by U (i.e., the Couette part of the film flow) does not contribute at all to the longitudinal pressure gradient $\Delta P/l$. Finally, the conservation of energy at the melting front requires that

$$k\frac{\Delta T}{\delta} \sim \rho_s h_{sf} V. \tag{24}$$

If we eliminate u and δ between Eqs. (22)–(24), we obtain a melting speed which can be nondimensionalized in the form of the Peclet number base on l,

$$\frac{Vl}{\alpha} \sim \left(\frac{\rho}{\rho_s}\mathrm{Ste}\right)^{3/4}\left(\frac{\Delta P \cdot l^2}{\mu\alpha}\right)^{1/4} \tag{25}$$

This scaling law reproduces exactly the plane contact melting result (20) if we set $l = L$ when $L \ll B$, and $l = B$ when $B \ll L$, i.e., when l represents the shorter of the two sides of the rectangular area of contact. More important, Eq. (25) also correlates the results for contact melting inside capsules and around embedded hot objects. First, we must recognize that the excess pressure scale ΔP can be defined as follows:

$$\Delta P = \frac{\text{the net weight of the object surrounded by liquid}}{\text{the horizontal projected area of that object}}. \tag{26}$$

In the case of melting inside capsules, the numerator represents the net *initial* weight of the solid phase-change material. Definition (26) yields $\Delta P = g\,\Delta\rho(\pi D/4)$ for a horizontal cylinder, and $\Delta P = g\,\Delta\rho(2D/3)$ for a sphere. The excess density of the sinking object is $\Delta\rho = \rho_s - \rho$ for melting inside a capsule (Fig. 1), and $\Delta\rho = \rho_0 - \rho$ for objects embedded in a solid phase-change material. The results on contact melting reviewed in Sections II and III can now be rewritten as follows:

Cylindrical capsule, horizontal [Fig. 1, Eq. (1) with $(1 + C) \cong 1$, and $\bar{V} = D/t_f$]:

$$\frac{\bar{V}D}{\alpha} = 1.015\frac{\rho}{\rho_s}\mathrm{Ste}^{3/4}\left(\frac{\Delta P \cdot D^2}{\mu\alpha}\right)^{1/4} \qquad (l = 0.971D). \tag{27}$$

Spherical capsule [Fig. 1, Eq. (5) with $\bar{V} = D/t_f$]:

$$\frac{\bar{V}D}{\alpha} = 1.297\frac{\rho}{\rho_s}\mathrm{Ste}^{3/4}\left(\frac{\Delta P \cdot D^2}{\mu\alpha}\right)^{1/4} \qquad (l = 0.595D). \tag{28}$$

Embedded horizontal cylinder [Fig. 3, Eq. (11)]:

$$\frac{VD}{\alpha} = 1.257\,\mathrm{Ste}^{3/4}\left(\frac{\Delta P \cdot D^2}{\mu\alpha}\right)^{1/4} \qquad (l = 0.633D). \tag{29}$$

Embedded sphere [Fig. 3, Eq. (9)]:

$$\frac{VD}{\alpha} = 1.682\,\mathrm{Ste}^{3/4}\left(\frac{\Delta P \cdot D^2}{\mu\alpha}\right)^{1/4} \qquad (l = 0.353D). \tag{30}$$

Equations (20) and (27)–(30) show that the scaling law (25) predicts within several percentage points the melting speed in all geometries if the length scale l is interpreted as the actual dimension of the projected area of contact (namely, D in Figs. 1 and 3, and $\min(L, B)$ in Fig. 4). There is some disagreement as to the role played by the density ratio ρ/ρ_s. Note that this ratio enters as $(\rho/\rho_s)^{3/4}$ in the scaling law (25), as ρ/ρ_s in the formulas (27)–(28) for melting inside capsules, while it is absent from the results (29)–(30) for melting around embedded hot objects. Numerically, however, the effect of ρ/ρ_s is very small, as it is close to 1. To the right of Eqs. (27)–(30) are the l values that would make these equations agree exactly with Eq. (25), again, if we discount the ρ/ρ_s effect. (By "exact" agreement we mean that the leading numerical factor on the right-hand side of Eqs. (27)–(30) is equal to 1.)

VI. Melting Due to Viscous Heating in the Liquid Film

At sufficiently high sliding velocities U, the slider temperature and the temperature difference across the film are dictated by viscous heating of the thin film. In this limit the conduction heat transfer absorbed by the melting front is balanced by the viscous heating effect, as shown by the last two scales of Eq. (14),

$$\alpha\frac{\Delta T}{\delta^2} \sim \frac{\mu}{\rho c_P}\left(\frac{U}{\delta}\right)^2, \tag{31}$$

so that now the temperature difference scale is

$$\Delta T \sim \frac{\mu}{k}U^2. \tag{32}$$

One interesting aspect of the ΔT scale is its independence of film thickness δ. The order of magnitude conservation statements for mass, momentum, and energy continue to be represented by Eqs. (22)–(24) in which $l \sim L$, and the ΔT scale is now furnished by Eq. (32).

By solving Eqs. (22)–(24) and (32), we obtain the melting speed V,

$$\frac{VL}{\alpha} \sim \left(\frac{\rho}{\rho_s} \text{Ste}_\mu\right)^{3/4} \left(\frac{\Delta P \cdot L^2}{\mu\alpha}\right)^{1/4}, \tag{33}$$

which looks like Eq. (25) except that Ste_μ is a new dimensionless group, namely, the Stefan number based on the viscous heating temperature rise (32),

$$\text{Ste}_\mu = \frac{c_P}{h_{sf}} \cdot \left(\frac{\mu}{k} U^2\right) = \Pr \frac{U^2}{h_{sf}}. \tag{34}$$

Equation (33) shows that when contact melting is due to viscous heating, the melting speed V is proportional to $U^{3/2}$. Recall that when viscous heating is negligible, as in Eq. (25), V is independent of U.

The film thickness scale retains the form encountered in Eq. (17), again, with Ste_μ in place of Ste,

$$\frac{\delta}{L} \sim \left(\frac{\rho}{\rho_s} \text{Ste}_\mu\right)^{1/4} \left(\frac{\Delta P \cdot L^2}{\mu\alpha}\right)^{-1/4}. \tag{35}$$

This shows that the film thickness increases as $U^{1/2}$, i.e., as the viscous heating effect intensifies. The δ scale is also proportional to $L^{1/2}$ and $\Delta P^{-1/4}$.

Finally, the friction coefficient scale is obtained by dividing the total friction force $F_t \sim \mu(U/\delta)BL$ by the total normal force $F_n = \Delta P BL$,

$$\mu_f \sim \frac{UL}{\alpha} \left(\frac{\rho}{\rho_s} \text{Ste}_\mu\right)^{-1/4} \left(\frac{\Delta P \cdot L^2}{\mu\alpha}\right)^{-3/4}. \tag{36}$$

This can be compared to Eq. (21) to demonstrate how the viscous heating effect alters the behavior of the friction coefficient. Specifically, in Eq. (36) the friction coefficient is proportional to $U^{1/2}$, whereas in Eq. (21) it is proportional to U. The dependence of μ_f on L and ΔP is the same in Eqs. (21) and (36), in other words, the impact of parameters L and ΔP is insensitive to the degree to which viscous heating sustains the melting and lubrication process.

The scaling trends outlined in this section agree with the more exact results delivered by the complete thin-film analysis based on assumptions (a), (b), and (e) of Section II, and $L \ll B$. This analysis and its solution are reported in [33]–[40], and show that, in addition to the order of magnitude
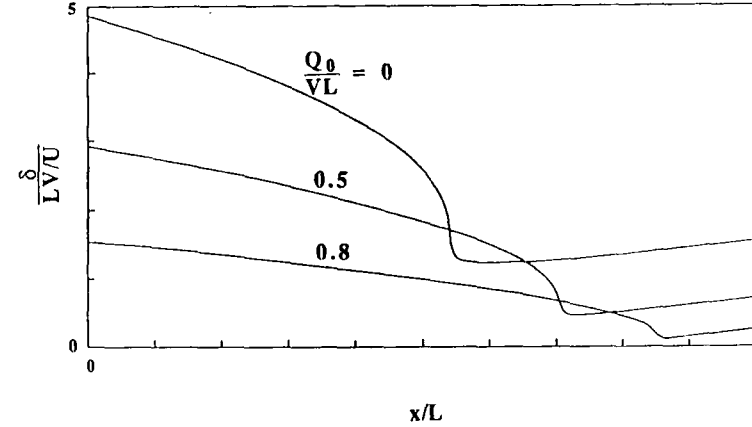
FIG. 6. Shape of relative motion gap when melting is driven by viscous heating in liquid film [40].

listed in Eq. (35), film thickness has the peculiar feature illustrated in Fig. 6. The relative motion gap is a converging-diverging channel with liquid squirting out through both ends. The slider moves to the right, so that $x = 0$ represents the upstream end and $x = L$ the downstream end. The curves are labeled according to the liquid flowrate Q_0 forced to the left through the $x = 0$ opening. This flowrate increases with the normal force (or $\Delta P = F_n/BL$) in the manner reported parametrically in Bejan [40].

The excess temperature between the slider (T_w) and the melting from (T_m) varies longitudinally as shown in Fig. 7. The hot spot is always on the slider and in the plane of its entrance to the contact region $(x = 0)$. The slider temperature increases as the $x = 0$ liquid flowrate increases, i.e., as the normal force increases.

VII. Lubrication by Melting Over Discrete Contact Spots

The results on melting and lubrication described in Sections IV–VI apply only when the mating surfaces are perfectly smooth so that the liquid film is continuous throughout the length L. Consider now the more likely situation in which the contact between solid phase-change material and a slider is made over a number of much smaller contact spots. Assume, as in Fig. 8, that the macroscopic surface (S) with which the solid phase-change material steps on the slider contains NS contact spots, where N is the number of contact spots per unit area. Assume, further that each contact spot has an area of order $L \times L$.
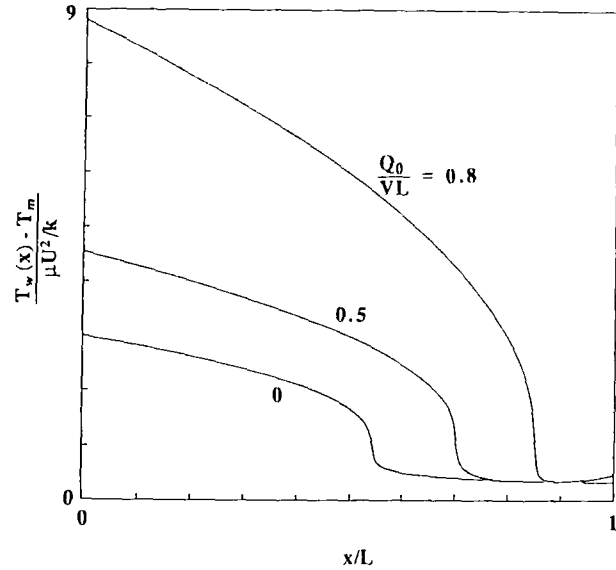
FIG. 7. Slider temperature when melting is driven by viscous heating in liquid film [40].
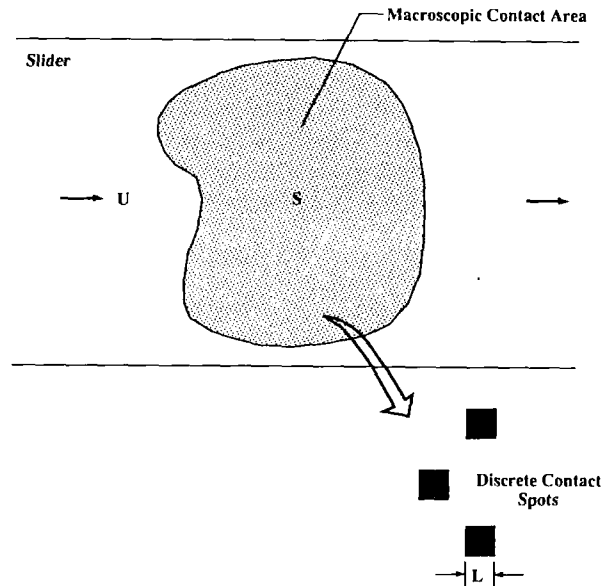

FIG. 8. Sliding, melting and lubrication over discrete contact spots (asperities).

Contact melting and lubrication occur over each contact spot. The challenge is to predict the friction coefficient between the "macroscopic" slider and the phase-change material,

$$\hat{\mu}_f = \frac{\hat{F}_n}{\hat{F}_t},\tag{37}$$

where $\hat{F}_n$ and $\hat{F}_t$ are the total normal and tangential forces shared over area S. The relations between these macroscopic forces and the forces shared through a single contact spot (F_n, F_t) are

$$\hat{F}_n = NSF_n \quad \text{and} \quad \hat{F}_t = NSF_t.\tag{38}$$

Dividing these relations, we find that the macroscopic friction coefficient $\hat{\mu}_f$ is the same as the microscopic (single spot) friction coefficient μ_f,

$$\hat{\mu}_f = \frac{NSF_n}{NSF_t} = \mu_f,\tag{39}$$

given by Eqs. (21) and (36). The excess pressure ΔP that appears in Eqs. (21) and (36) can be related to the known (externally imposed) normal force $\hat{F}_n$ by writing

$$\Delta P \cdot L^2 = F_n = \frac{\hat{F}_n}{NS}.\tag{40}$$

In this way the macroscopic coefficient can be estimated, provided we know the total normal force $\hat{F}_n$, number of contact spots NS, and the microscopic length scale L. Some of these parameters are not independent of each other if the asperities (contact spots) experience plastic deformation. If H is the microhardness of the softer of the two solids (most likely the phase-change material), then the total area of actual contact $(NS \cdot L^2)$ and the macroscopic area (S) are in the following proportion:

$$\frac{NSL^2}{S} = \frac{\hat{F}_n/S}{H}.\tag{41}$$

On the right-hand side, $\hat{F}_n/S$ is the apparent (macroscopic) pressure imposed over the macroscopic area S. Equation (41) is widely used for the purpose of estimating heat transfer through discrete points of thermal contact (Yovanovich [43-45], Fletcher [46], and Bejan [47]). In conclusion, on the right-hand side of Eqs. (21) and (36) the product $\Delta P \cdot L^2$ is replaced by $H \cdot L^2$ (cf. Eq. (41)),

$$\Delta P \cdot L^2 = \frac{\hat{F}_n}{NS} = H \cdot L^2\tag{42}$$

The microscopic length scale L, which is needed for calculating the Peclet number UL/α in Eqs. (21) and (36), can be estimated based on Eq. (41) when the asperities density N is known.

VIII. The Effect of Heat Transfer in the Solid Parts

The assumptions that in Fig. 4 the slider is isothermal (T_w) and the solid phase-change material is isothermal at the melting point (T_m) were relaxed in a more recent study by Litsek and Bejan [48]. With reference to the two-dimensional ($B \gg L$) melt lubrication geometry of Fig. 9, they showed that when the two solid parts are not isothermal, the melting rate and tangential force are substantially less.

Litsek and Bejan's analysis [48] is based on a conjugate thermal boundary layer model in which a solid block of phase-change material is subcooled ($T_0 < T_m$), the slider is hot ($T_s > T_m$), and the thermal diffusivities of the two solid parts (α_0 and α_s) are finite. The thickness of the thermal boundary layer in the solid phase-change material (δ_0) is independent of x, as the flow of this material into the boundary layer is independent of longitudinal position (V).
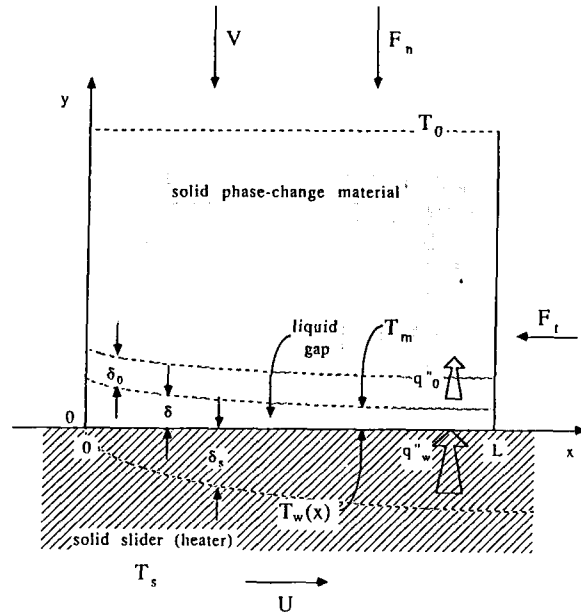
This feature also controls the distribution of heat flux on the slider surface. Here the distribution is uniform, q''_w, and the slider thermal boundary layer has the shape sketched in Fig. 9. In the end, the two thermal boundary layer solutions are matched to the solution for the flow and temperature in the lubricating film, where the viscous heating effect is assumed negligible.

The film thickness δ decreases in the U direction, unlike in Section IV where δ was uniform. It has the shape illustrated in Fig. 9, and is expressed analytically by

$$\frac{\delta}{L} = q\frac{U}{V} - p\left(\frac{x}{L}\right)^{1/2}. \tag{43}$$

The dimensionless numbers p and q are defined by

$$p = 1.13\frac{k}{k_s}\left(\frac{UL}{\alpha_s}\right)^{1/2}, \tag{44}$$

$$q = \frac{k(T_s - T_m)}{\rho_0 h_{sf}UL(1 + \text{Ste})}, \tag{45}$$

where Ste is the solid subcooling Stefan number, $\text{Ste} = c_0(T_m - T_0)/h_{sf}$, k_s is the thermal conductivity of the slider at T_s, and ρ_0 and c_0 are the properties of the solid phase-change material at T_0. Table I shows the order

FIG. 9. Thermal boundary layers formed in the solid parts sliding with melt lubrication [48].

TABLE I

NUMERICAL EXAMPLES OF SLIDING-MELTING CONFIGURATIONS AND ORDER OF MAGNITUDE OF DIMENSIONLESS PARAMETERS p AND q (IN ALL THE EXAMPLES $U = 1$ CM/S AND $L = 10$ cm)

| Property	Units	Ice on steel	Polymer on steel	Zinc on steel	Tin on steel
k	(W/m °C)	0.55	0.178	56.9	33.5
h_{sf}	(J/kg)	334,944	130,000	102,138	60,697
α_0	(m²/s)	4.7×10^{-5}	9×10^{-8}	4.2×10^{-5}	6.3×10^{-5}
ρ_0	(kg/m³)	922	760	7140	7304
c_0	(J/kg °C)	2009.7	2600	388	139
k_0	(W/m °C)	87.44	0.178	116	64
α_s	(m²/s)	1.5×10^{-5}	1.5×10^{-5}	1.5×10^{-5}	1.5×10^{-5}
k_s	(W/m °C)	55	55	55	55
T_s	(°C)	30	$180 \to 280$	$450 \to 500$	$250 \to 350$
T_m	(°C)	0	110	419	231
T_0	(°C)	-30	$20 \to 80$	$30 \to 400$	$30 \to 200$
p		29	9.4	3001	1775
q		4.5×10^{-6}	$4.5 \times 10^{-6} \to$ 6.6×10^{-5}	$1.3 \times 10^{-4} \to$ 5.8×10^{-4}	$1 \times 10^{-6} \to$ 8.4×10^{-6}
References		[49–51]	[52]	[53]	[53]
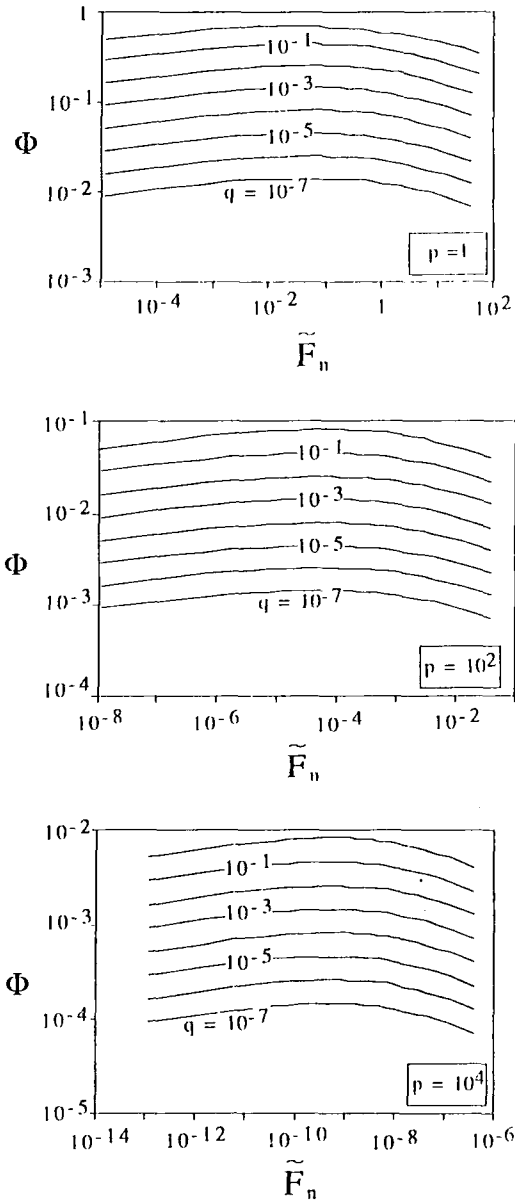
of magnitude of the two numbers p and q. The isothermal slider surface limit corresponds to $p \to 0$.

The resulting expression for the melting speed V is

$$\frac{V}{U} = \tilde{F}_n^{1/4} q^{3/4} \Phi \tag{46}$$

where the dimensionless normal force group is defined as

$$\tilde{F}_n = \frac{F_n}{\mu UB}. \tag{47}$$

The dimensionless factor Φ is a function of $\tilde{F}_n$, p and q, as shown in Fig. 10. The Φ factor equals 1 in the limit $p \to 0$, when Eq. (46) becomes identical to Eq. (20). Figure 10 shows that Φ decreases steadily as p increases, i.e., as the slider departs from the isothermal-wall description. According to Eq. (46), as Φ becomes considerably smaller than 1, the melting speed becomes considerably smaller than the value in the isothermal slider limit.

The net tangential force between the two bodies is expressed by

$$\frac{F_t}{\mu UB} = \tilde{F}_n^{1/4} q^{-1/4} \Psi. \tag{48}$$

The factor $\Psi(\tilde{F}_n, p, q)$ is reported in Fig. 11, which shows that Ψ approaches 1 as $p \to 0$. In the same limit, Eq. (48) approaches the isothermal-slider result for F_t presented in Eq. (21). Since the factor Ψ is less than 1, the tangential force is less than the F_t value calculated in the isothermal slider limit.

IX. Rolling Contact Melting

The "line" of rolling contact between a cylinder of solid phase-change material (the roller) and a plane heater (the base) can also be wetted by a film of liquid phase-change material. A similar film can occur between a cylindrical heater (roller) and a plane solid phase-change material (base). The first of these configurations is sketched in Fig. 12, which illustrates the normal force F_n, tangential force F_t, torque M, temperature difference $\Delta T = T_s - T_m$, and geometric and thermophysical properties. The liquid film has a shape similar to that sketched in the figure. The solid phase-change material is at the melting point (T_m) and the flat heater is isothermal at T_s.

The chief unknown is the melting speed $V = -dr/dt$, where r is the instantaneous radius of the phase-change roller. Note that in Fig. 12 the Cartesian system (x, y) is attached to the base surface and that the y axis
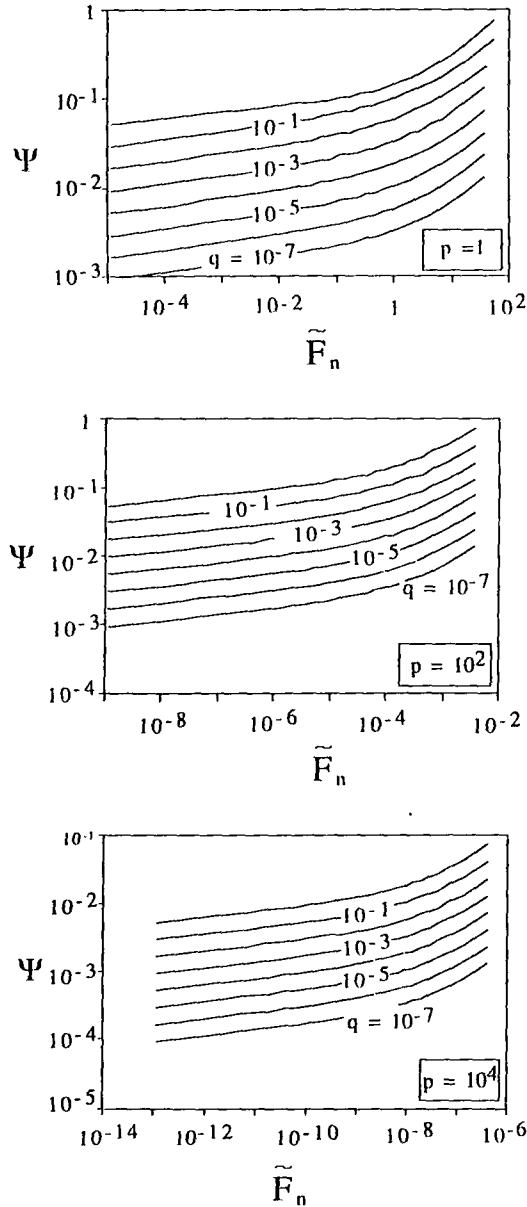

FIG. 10. Correction factor Φ for effect of lateral conduction on melting speed during sliding with melt lubrication [48].

FIG. 11. Correction factor Ψ for effect of lateral conduction on tangential force during sliding with melt lubrication [48].
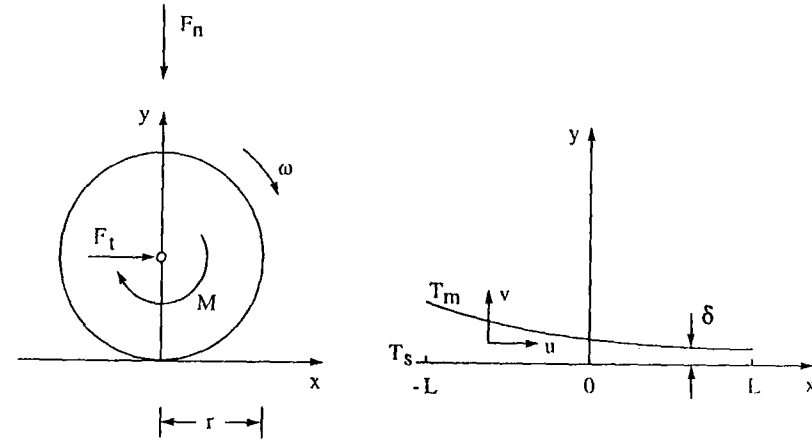

FIG. 12. Cylinder of solid phase-change material rolling on flat heater. On right side, an enlargement of the rolling contact region and the liquid film [54].

passes through the center of the roller. Bejan [54] developed a method for calculating the melting speed when the melt lubrication phenomenon is analogous to that analyzed in Section IV, i.e., when viscous heating of the film is negligible. The solution for V can be reduced to a relation between only four dimensionless groups:

$$f(F_{n*}, F_{t*}, M_*, B) = 0, \tag{49}$$

in which the first three groups are the dimensionless normal force, tangential force, and torque applied on the roller,

$$F_{n*} = \frac{F_n'}{\mu \omega r}, \tag{50}$$

$$F_{t*} = \frac{F_t'}{\mu \omega r}, \tag{51}$$

$$M_* = \frac{M'}{\mu \omega r^2}, \tag{52}$$

The primes indicate that F_n', F_t' and M' are expressed per unit cylinder length, i.e., in the direction perpendicular to the plane of Fig. 12. The fourth group (B) is the characteristic heat transfer parameter of the rolling contact process,

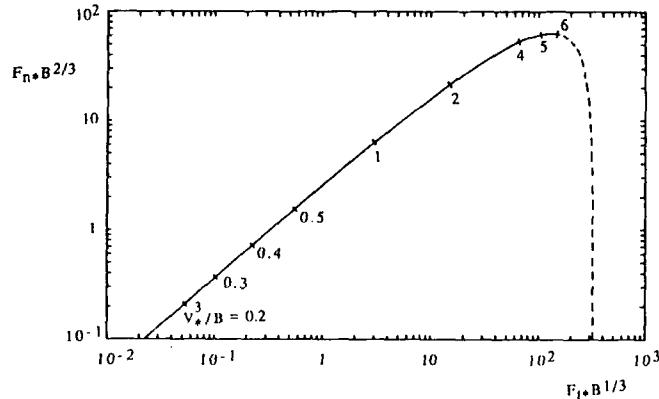$$B = \frac{k(T_s - T_m)}{\rho h_{sf} \omega r^2}, \tag{53}$$

FIG. 13. Melting speed of a cylinder mounted freely on its axle [54].

and should not be confused with the transversal dimension in Fig. 5. In addition to V, the angular speed ω and the film length $2L$ are also unknown, since they cannot be specified independently in F_n', F_t', M', ΔT and all the properties are already known. The same can be said about the slip speed U (not shown in Fig. 12), which is the velocity of the base surface in the negative x direction.

When the roller is mounted freely on its axle, the torque is zero and the number of dimensionless groups in Eq. (49) drops to 3. One more degree of freedom disappears when (i) the film length L is much less than the roller radius r, and (ii) the film is slender, $\delta \ll L$. These two conditions require
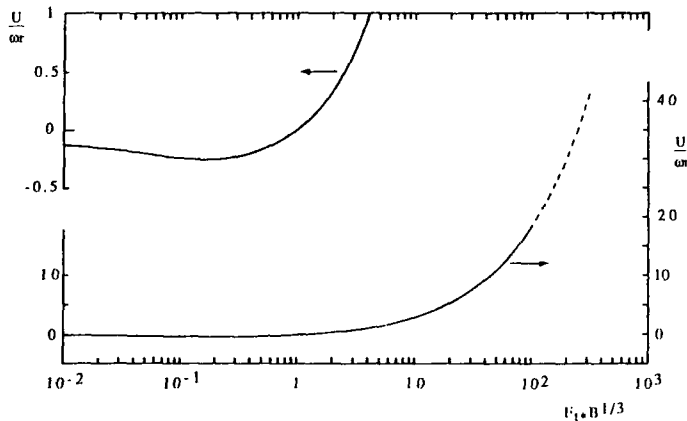

FIG. 14. Slip speed between bottom of the phase-change roller and flat heater, with roller mounted freely on its axle [54].

simultaneously that

$$B^{1/2} \ll V_* \ll 1, \tag{54}$$

where V_* is the dimensionless melting speed,

$$V_* = \frac{V}{\omega r}. \tag{55}$$

With only two dimensionless degrees of freedom left, the solution (49) can be represented as a plane curve. Figure 13 shows the relation between the normal force ($F_{n*}B^{2/3}$) and tangential force ($F_{t*}B^{1/3}$), and the relation between the melting speed (V_*^3/B) and one of the two forces. This solution expires when V_*^3/B is roughly greater than 6. In the opposite extreme, where V_*^3/B is less than 1, the solution of Fig. 13 behaves as

$$F_{n*}B^{2/3} = \frac{1728}{175}\left(\frac{V_*^3}{B}\right)^{7/3}, \tag{56}$$

$$F_{t*}B^{1/3} = \frac{736}{175}\left(\frac{V_*^3}{B}\right)^{8/3}. \tag{57}$$

Physical quantities of interest, such as the melting speed V and the angular speed ω, can be deduced from the dimensionless solution by recognizing the definitions of the dimensionless parameters. One further example is presented in Fig. 14, which shows the slip speed as the group $U/\omega r$ versus the tangential force parameter used also on the abscissa of Fig. 13.

Figures 15 and 16 summarize the results for the case in which the roller is stationary, i.e., the cylinder axis does not move along the flat heater.
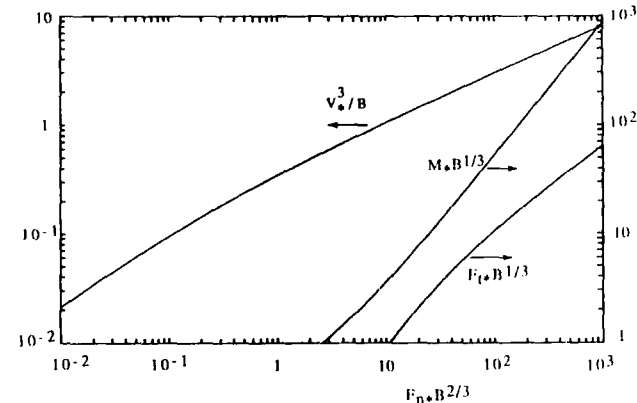

FIG. 15. Solution for rolling contact melting of stationary cylinder [54].